

7-2023

Hypo-Osmotic Stress and Pore-Forming Toxins Adjust the Lipid Order in Sheep Red Blood Cell Membranes

Rose Whiting
Boise State University

Sevio Stanton
Boise State University

Maryna Kucheriava
Boise State University

Aviana R. Smith
Boise State University

Matt Pitts
Boise State University

See next page for additional authors

Authors

Rose Whiting, Sevio Stanton, Maryna Kucheriava, Aviana R. Smith, Matt Pitts, Daniel Robertson, Jacob Kammer, Zhiyu Li, and Daniel Fologea

Article

Hypo-Osmotic Stress and Pore-Forming Toxins Adjust the Lipid Order in Sheep Red Blood Cell Membranes

Rose Whiting^{1,2}, Sevio Stanton¹, Maryna Kucheriava¹, Aviana R. Smith¹ , Matt Pitts^{1,2}, Daniel Robertson¹, Jacob Kammer^{1,3}, Zhiyu Li¹ and Daniel Folegea^{1,2,*}

¹ Department of Physics, Boise State University, Boise, ID 83725, USA

² Biomolecular Sciences Graduate Program, Boise State University, Boise, ID 83725, USA

³ Department of Family Medicine, Idaho College of Osteopathic Medicine, Meridian, ID 83642, USA

* Correspondence: danielfolegea@boisestate.edu

Abstract: Lipid ordering in cell membranes has been increasingly recognized as an important factor in establishing and regulating a large variety of biological functions. Multiple investigations into lipid organization focused on assessing ordering from temperature-induced phase transitions, which are often well outside the physiological range. However, particular stresses elicited by environmental factors, such as hypo-osmotic stress or protein insertion into membranes, with respect to changes in lipid status and ordering at constant temperature are insufficiently described. To fill these gaps in our knowledge, we exploited the well-established ability of environmentally sensitive membrane probes to detect intramembrane changes at the molecular level. Our steady state fluorescence spectroscopy experiments focused on assessing changes in optical responses of Laurdan and diphenylhexatriene upon exposure of red blood cells to hypo-osmotic stress and pore-forming toxins at room temperature. We verified our utilized experimental systems by a direct comparison of the results with prior reports on artificial membranes and cholesterol-depleted membranes undergoing temperature changes. The significant changes observed in the lipid order after exposure to hypo-osmotic stress or pore-forming toxins resembled phase transitions of lipids in membranes, which we explained by considering the short-range interactions between membrane components and the hydrophobic mismatch between membrane thickness and inserted proteins. Our results suggest that measurements of optical responses from the membrane probes constitute an appropriate method for assessing the status of lipids and phase transitions in target membranes exposed to mechanical stresses or upon the insertion of transmembrane proteins.

Keywords: lipid order; hypo-osmotic shock; pore-forming toxins; Laurdan; diphenylhexatriene; phase transition



Citation: Whiting, R.; Stanton, S.; Kucheriava, M.; Smith, A.R.; Pitts, M.; Robertson, D.; Kammer, J.; Li, Z.; Folegea, D. Hypo-Osmotic Stress and Pore-Forming Toxins Adjust the Lipid Order in Sheep Red Blood Cell Membranes. *Membranes* **2023**, *13*, 620. <https://doi.org/10.3390/membranes13070620>

Academic Editors: Oleg Kovtun and Jerry C. Chang

Received: 5 April 2023

Revised: 7 June 2023

Accepted: 22 June 2023

Published: 25 June 2023



Copyright: © 2023 by the authors. Licensee MDPI, Basel, Switzerland. This article is an open access article distributed under the terms and conditions of the Creative Commons Attribution (CC BY) license (<https://creativecommons.org/licenses/by/4.0/>).

1. Introduction

The cell membrane evolved from a selective barrier separating the cell from the external environment to a more complex functional structure with regulatory roles in transport, communication, and signal transduction. The ingenious arrangement of lipids proposed by the long-revered mosaic fluid model more than five decades ago is still the most fundamental model for the structure and dynamics of the plasma membrane [1]. The concept of basic lipid state phases postulated by the original model (i.e., liquid crystalline and bilayer) [2] has been refined [1,3–6] to better capture the importance of lipid organization in domains [7–12] for describing the membrane's dynamics, regulation, and permeation. Currently, the membrane is viewed as a complex system consisting of liquid-ordered and liquid-disordered phases [5,13]. The lipid order in the membranes has physiological relevance for a large variety of fundamental biological processes: apoptosis [14], signaling [15–18], cellular development [19], interactions [20], receptor stabilization [21], the segregation and mobility of membrane proteins [22], microvesicle release [23], and clonal

expansion [24]. Consequently, the assessment of changes in lipid ordering is under intense scrutiny to identify the origin of triggering factors and the cascades of biochemical and biophysical signals leading to the observed biological effects. Investigations into the organization of lipids in membranes may be experimentally approached by employing numerous biophysical techniques. Despite the variety of methodologies, the large availability of steady-state fluorescence spectroscopy instrumentation and the ease of experimental procedures led to a wide adaptation of this technique for investigating the status of membranes in natural and artificial systems [25–32].

Multiple fluorescent probes for evaluating membrane status and lipid organization are commonly used, and many alternatives have been proposed for adoption. Among these, 6-dodecanoyl-2-dimethylaminonaphthalene (Laurdan) and 1,6-diphenyl-1,3,5-hexatriene (DPH) have been extensively used as reporters in numerous natural and artificial membrane systems [26,27,33–38]. While neither probe directly responds to lipid ordering, their optical responses adjust to changes in the physical environment. Laurdan's dipolar relaxation leads to spectral shifts [5,30–32,34,38,39], and DPH's anisotropy is affected by the rotational diffusion of the dye [29,36,37]. Both mechanisms are influenced by the ordering of the lipids in the membranes in which the probes reside.

Changes in membrane status are ascribed to adjustments in numerous physical and biomechanical parameters, which are closely associated with lipid ordering [25,40–46]. Absolute lipid ordering is not easy to quantify. As a result, many investigations focused on assessing its variation in response to physical and chemical adjustments. The most common environmental stressor is temperature as changes in ordering are closely related to temperature-induced phase transitions. Temperature-induced phase transitions are easier to observe in artificial systems with limited components [27,28,47] and intervals that include the melting temperature of the lipids under investigation [26–28,47,48]. The indicative hallmark of transitions from ordered to disordered states is the sigmoidal shape of the melting curve [26–28]. Even in artificial systems, the addition of cholesterol dramatically changes the transition profile by adjusting the melting temperature and flattening the melting curve. Consequently, sigmoidal shapes may be observed only by pushing the temperatures well beyond physiological ranges [27,28,47]. The situation is more complicated for cell membranes, in which the composition is very complex [49,50] and may include stabilizing small molecules. Natural membranes are predominantly in a liquid-ordered phase and unable to attain an ordered gel phase within physiological temperature ranges [2]. Cholesterol additions adjust the melting temperatures and smooth the transitions as a result of lipid ordering elicited by cholesterol [26,28,51,52]. However, this makes data interpretation difficult. One example comes from attempts to decipher the effects of osmotic pressure on membrane properties. In this respect, several reports indicate specific changes in lipid ordering, but these investigations employed either artificial membranes or hyperosmotic shock [35,53–55]. These experiments demonstrated that hyperosmotic conditions lead to increased rigidity, ordering, and transition temperature, while hypo-osmotic shock experiments that employed *S. cerevisiae* show membrane fluidization [56]. In addition to assessing the effects of environmental factors, a different direction of research focuses on understanding the effects on ordering of various inclusions into membranes, which is highly relevant for protein insertion, assembly, and biological functionalities.

Despite numerous advancements in establishing relationships between the influence of physical, chemical, and biological factors on lipid organization and biological consequences, little is known of the influence of hypo-osmotic pressure or the insertion of transmembrane proteins on ordering in natural membranes. To fill these gaps in our knowledge, we employed fluorescence techniques to measure optical responses of Laurdan and DPH on red blood cell (RBC) membranes exposed to hypo-osmotic shocks and increasing concentrations of pore-forming toxins (PFTs).

We concluded that hypo-osmotic shocks and PFTs acting at room temperature gradually decrease the lipid ordering to an extent comparable with what is customarily observed for phase transitions. The effects of hypo-osmotic shocks are interpreted by considering the

stretching of the membranes, while the effects of protein insertions are explained based on local changes in geometry and bending resulting from hydrophobic mismatches.

2. Materials and Methods

2.1. Red Blood Cell Preparation

Freshly isolated sheep RBCs in Alsever's solution (Colorado Serum Company, Denver, CO, USA) were utilized in our experiments. The RBCs were purified by repeated centrifugation (3500 RPM, five minutes, Fisher Scientific bench centrifuge, ThermoFisher Scientific, Waltham, MA, USA) and washing in phosphate buffer saline (PBS, pH 7.2), followed by a final suspension in PBS. The RBCs in the final suspension were counted with a bench cytometer (ThermoFisher Scientific, Waltham, MA, USA) and provided a density of $\sim 6 \times 10^9$ cells/mL. The RBCs were kept on ice but brought to room temperature before initiating the experiments. The RBCs were stained with Laurdan or DPH (both from ThermoFisher Scientific, Waltham, MA, USA) for fluorescence measurements. Laurdan and DPH powders were solubilized at 1 mM final concentration in DMSO (Sigma-Aldrich, St. Louis, MO, USA). For complete solubilization, the mixtures were vigorously vortexed, followed by bath sonication for ten minutes. The stock solutions were kept away from direct light and exposed to additional vortexing and one minute of sonication before each use. For experiments employing fluorescence measurements, 2 mL of RBC stock solution were stained with Laurdan or DPH at 5 μ M final concentration, rotated in a test tube for two hours at room temperature, and washed three times with PBS by centrifugation. The final pellet was reconstituted in 2 mL PBS, and aliquots from it were used for cholesterol extraction, exposure to hypo-osmotic shock, and exposure to pore-forming toxins. Multiple 2 mL tubes of stained and non-stained RBC stocks were prepared when larger volumes were needed for experiments. In this case, all the pristine stocks were mixed prior to staining and/or experimentation to avoid non-uniformities in each sample's cellular density.

To deplete the cholesterol in the RBC membranes, we used methyl- β -cyclodextrin [48] (MBCD, Sigma-Aldrich, St. Louis, MO, USA) solubilized in PBS at 250 mM final concentration. The stock solution was briefly sonicated for 30 s before each use in a bath sonicator. Cholesterol extraction from RBCs was performed by combining in test tubes PBS, 25 μ L stock of stained RBCs, and MBCD at final concentration ranging from 0 μ M (control) to 1000 μ M for a total volume of 3 mL. The tubes were rotated in a bench rotator at room temperature for two hours, and the contents were transferred to plastic cuvettes (1 cm path length) for fluorescence measurements.

2.2. Pore-Forming Toxins

Two PFTs, lysenin and streptolysin O (SLO), were used for our experiments. Aliquots from a stock solution of oxygen-stable SLO (a kind gift from Dr. Sarah Hobdey, VA, Boise, ID, USA) were serially diluted in PBS to achieve the desired concentrations such that no more than a few μ L were added to the RBC solutions. The final concentrations of lysenin and SLO in the samples are indicated in the Results and Discussion. Aliquots from a recombinant lysenin stock solution [57] were serially diluted similarly to SLO. Both toxins were added to test tubes containing 3 mL of PBS and 25 μ L stock of stained RBCs. PFT-exposed samples and negative controls without PFTs were rotated for one hour at room temperature in a bench rotator, transferred to cuvettes, and subjected to fluorescence measurements.

2.3. Hypo-Osmotic Shock Exposure

A total of 25 μ L of stained stock RBCs were added to test tubes containing 3 mL mixtures of PBS and water to achieve the desired hypo-osmotic pressures. The percentages of added water varied from 0% (control) to 80%. After the tubes were rotated for 20 min in a bench rotator at room temperature, the solutions were transferred to cuvettes for fluorescence measurements.

2.4. Fluorescence Measurements

The fluorescence was measured with a Fluoromax 4 Spectrofluorometer (Horiba Scientific, Piscataway, NJ, USA). To ensure maximum sensitivity and minimization of experimental errors, we implemented measurement protocols consisting of single-point excitation and one- or two-point emission. For Laurdan, the protocol was defined as follows: 410 nm excitation, 5 nm excitation bandpass, emission one at 440 nm, 10 nm emission bandpass, emission two at 490 nm, 10 nm emission bandpass, and a target measurement error of 1%. Although Laurdan is customarily excited at 350 nm, excitation at longer wavelengths improved the signal/noise ratio, which is theorized to be a consequence of photo-selection [25,31,34]. All fluorescence intensity measurements were carried out in triplicate and at room temperature. The generalized polarization function (GP) was estimated from the ratiometric formula [4,30,33,47,58]:

$$GP = \frac{I_{440} - I_{490}}{I_{440} + I_{490}} \quad (1)$$

The GP values were computed directly in the instrument's software. Average values and standard deviations were calculated and plotted using Origin 8.5.2 software package (OriginLab, Northampton, MA, USA). Anisotropy was measured with the same instrument equipped with polarizers to determine the fluorescence intensity for the parallel (I_{\parallel}) and perpendicular (I_{\perp}) orientations. The anisotropy parameter "p" was measured with the single-point protocol (360 nm excitation, 5 nm bandpass, 450 nm emission, 10 nm bandpass, and 1% error) from the following relation [14,38,59]:

$$p = \frac{I_{\parallel} - I_{\perp}}{I_{\parallel} + 2I_{\perp}} \quad (2)$$

The sigmoidal plots have been fitted in Origin 8.5.2 with the four-parameter Boltzmann function [26,28]:

$$y = \frac{\max - \min}{1 + e^{(x-x_0)/dx}} + \min \quad (3)$$

where max and min are the y coordinates of the plateaus, x_0 is the x-coordinate of the inflex points, and dx is the slope of the corresponding dependence [28].

3. Results and Discussion

3.1. Cholesterol Depletion in Red Blood Cell Membranes Modulates Lipid Ordering

Our initial investigations focused on understanding the response to cholesterol reduction in RBC membranes at room temperature by gradual depletion with MBCD. The effects of the cholesterol content adjustments in artificial and natural membranes have been extensively investigated with respect to the changes in the optical response of membrane probes [26–29,31,33,60,61]. Many of these experiments were interpreted by exploiting the changes elicited over substantial variations in temperature. We utilized these interpretations to relate the status of the membrane to molecular adjustments of the lipids in response to environmental factors excluding temperature as a variable parameter.

Figure 1 shows Laurdan's generalized polarization and DPH's anisotropy for RBCs exposed to increasing concentrations of MBCD (up to 1000 μ M). The control, 0 μ M of MBCD, was characterized by initial values of GP (\sim 0.6) and p (\sim 0.3) typical for artificial and natural membranes at room temperature [26–32,38,47,48,62]. To interpret the effects of cholesterol, we considered the changes in lipid ordering induced by temperature variations in membranes undergoing phase transitions [26,28,31,32,38,47].

Artificial membrane systems comprising few lipid components with no cholesterol exist in a highly ordered gel phase at low temperature (i.e., under the melting temperature). The increase in temperature leads to melting and the attainment of a liquid-disordered phase, and a clear order–disorder transition is easily observable within narrow temperature ranges [26–30,47,48,63]. The addition of cholesterol prevents the gel phase at temperatures

under the melting point, keeping the lipids in a liquid-ordered phase. Complete phase transitions can still be observed in complex artificial and natural membranes with cholesterol, but extreme temperature ranges must be employed [26,28,30,33]. For limited temperature intervals, the mostly linear variation of the optical response prevents ascribing a clear-cut transition temperature while enabling a qualitative analysis in terms of increasing or decreasing ordering [27,28,33].

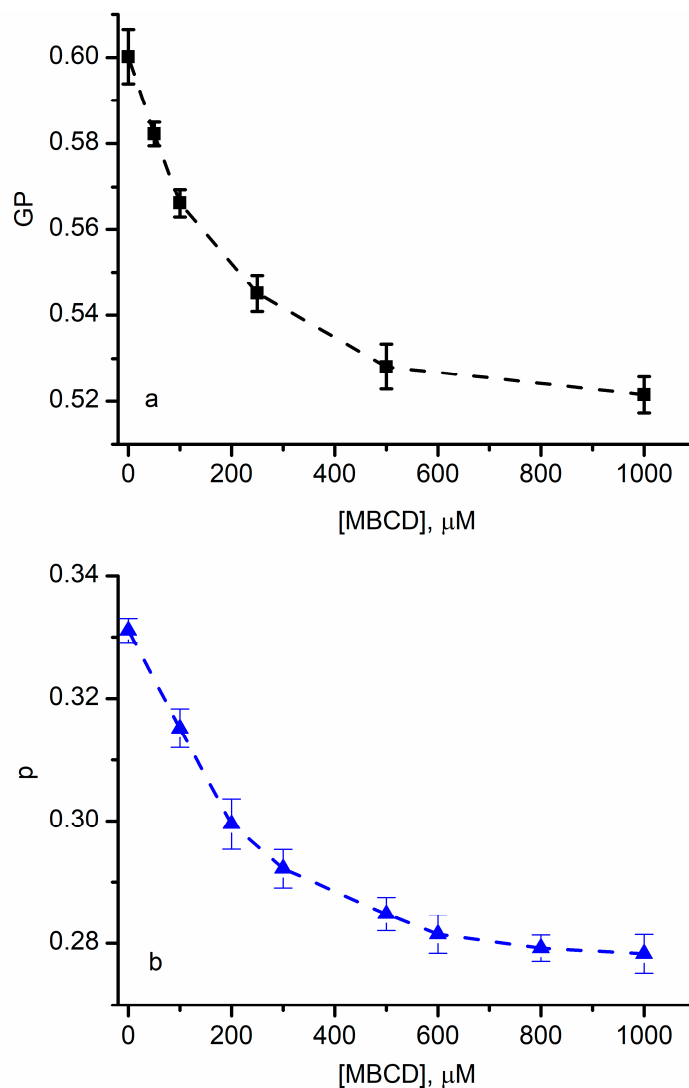


Figure 1. Cholesterol depletion in red blood cell (RBC) membranes adjusts the lipid ordering. The decrease in Laurdan's generalized polarization function (a) and anisotropy of diphenylhexatriene (DPH) (b) upon methyl- β -cyclodextrin (MBCD) addition indicates a reduced lipid order in the membranes. The symbols represent average values \pm SD ($n = 3$); the interrupted lines are added as visual aids.

At room temperature, RBCs are in a liquid-ordered phase, and the extraction of cholesterol is expected to lead to changes in ordering, which translates to changes in the GP and p parameters. We observed that both parameters decreased as the MBCD concentration increased, suggesting that cholesterol depletion led to a reduced order of the lipids in the membrane [4,14,26,28,48].

The determined changes in GP and p were small. However, large variations for similar MBCD concentrations have been obtained only in response to significant changes in temperatures when true phase transitions were recorded [26,48]. If we inspect these prior experiments, we may observe that the reported changes in GP and p near room temperature

are similar to our measurements. An additional contributor to these small variations is the fact that 1000 μM of MBCD does not completely remove the cholesterol from the target membranes, resulting in a large fraction of the initial cholesterol concentration still residing in the RBC membranes [48].

Our plots show a monotonic decrease in lipid ordering, but none suggest that a true phase transition occurred at room temperature due to cholesterol depletion since the typical sigmoidal shape of the plots [26–28,47,48,63] is not present. Despite the minor changes in GP and p, we can provide an interpretation of our data by accounting for effects of cholesterol at the molecular scale. Although no complete order–disorder transition is observed, and the degree of ordering cannot be determined, both results are consistent with a gradual reduction in the ordering of the lipids (i.e., the lipids become more disordered when the amount of cholesterol decreases). While the DPH's anisotropy is directly linked to viscosity and fluidity [27,28,36,38,48], the GP parameter is descriptive of dipolar relaxation [5,31,32,34,38,60]. Irrespective of the interpretation of the changes in GP upon cholesterol depletion (i.e., water penetration as opposed to the influence of the internal motions of lipids on the dipolar relaxation in the vicinity of the excited state dipole [25]), the shift in emission and the changes in anisotropy suggest a decrease in ordering.

3.2. Hypo-Osmotic Shock Modulates the Optical Responses of Environment-Sensitive Membrane Probes

Our next experiments focus on investigating the physical changes in lipids in cell membranes exposed to hypo-osmotic shock conditions. These investigations filled a large gap in our knowledge [53] in regard to lipid organization since prior explorations employed artificial membrane systems [35,54–56,64], hyperosmolarity [53,56], or temperature variations [56]. These experiments built a solid foundation for qualitative analyses of membrane status from the provided interpretations of the changes in the properties of membranes exposed to differential osmotic pressure conditions [55,56,65]. Laurdan and DPH in RBCs' membranes showed similar patterns in the optical responses upon exposure to hypo-osmotic conditions with respect to changes in generalized polarization and anisotropy (Figure 2).

The changes in GP and p are much larger than what we measured for cholesterol-depleted RBC membranes. The GP value decreased from ~ 0.6 to ~ -0.1 (theoretical range $+1:-1$), and DPH's anisotropy decreased from ~ 0.28 to ~ 0.02 (theoretical range $+1:0$). Both variations are typical for temperature-induced phase transitions [26,28,30,33,48]. For comparison, experiments on giant vesicles and yeast exposed to osmotic pressure conditions exhibited much smaller variations [35,56]. In addition to the large variation of the optical response recorded for RBCs under hypo-osmotic conditions, it was striking that the plots present a pronounced sigmoidal shape resembling true phase transitions similar to the ones determined for membrane systems undergoing significant temperature changes. The resemblance to phase transitions prompted us to apply a Boltzmann fit (Equation (3)) of the experimental data [26,28] to provide insight into the molecular processes accompanying changes in membranes exposed to hypo-osmotic pressure. The fit provided similar halfway values of the osmotic pressure (i.e., $\sim 35\%$ water for Laurdan and $\sim 42\%$ water for DPH). However, the Boltzmann fit is usually employed to provide an assessment of phase transitions and ordering induced by changes in temperature, and the determined halfway values indicate the temperatures at which a transition occurs [26,28]. This strongly suggests that hypo-osmotic pressure induces a major transition from liquid-ordered to liquid-disordered membranes at room temperature. One may argue that the asymptotic plateau observed at extreme hypo-osmotic conditions may be a consequence of complete membrane disintegration. However, membrane resealing after a rupture caused by hypo-osmotic shock is well documented [66,67], and our images (Supplementary Material) suggest the existence of intact membranes after applying hypo-osmotic shocks and PFT treatments. To explain this unexpected behavior in membranes containing cholesterol, we accounted for the potential relationships between lipid order, fluidity, and interactions in the membrane.

Basically, all the intermolecular forces between the components of the membrane have a short range [68]. Hypo-osmotic pressure leads to water transport into RBCs, swelling, increased membrane tension, an increased surface area, and an increase in the intermolecular distances [44,52,55,65,68–70] (as depicted in Figure 3). Consequently, the intermolecular forces were diminished dramatically because of their strong dependency on distance, the lipid order decreased, and the membrane became more fluid, which opposed what was observed for cells exposed to hyperosmotic pressure [53,56].

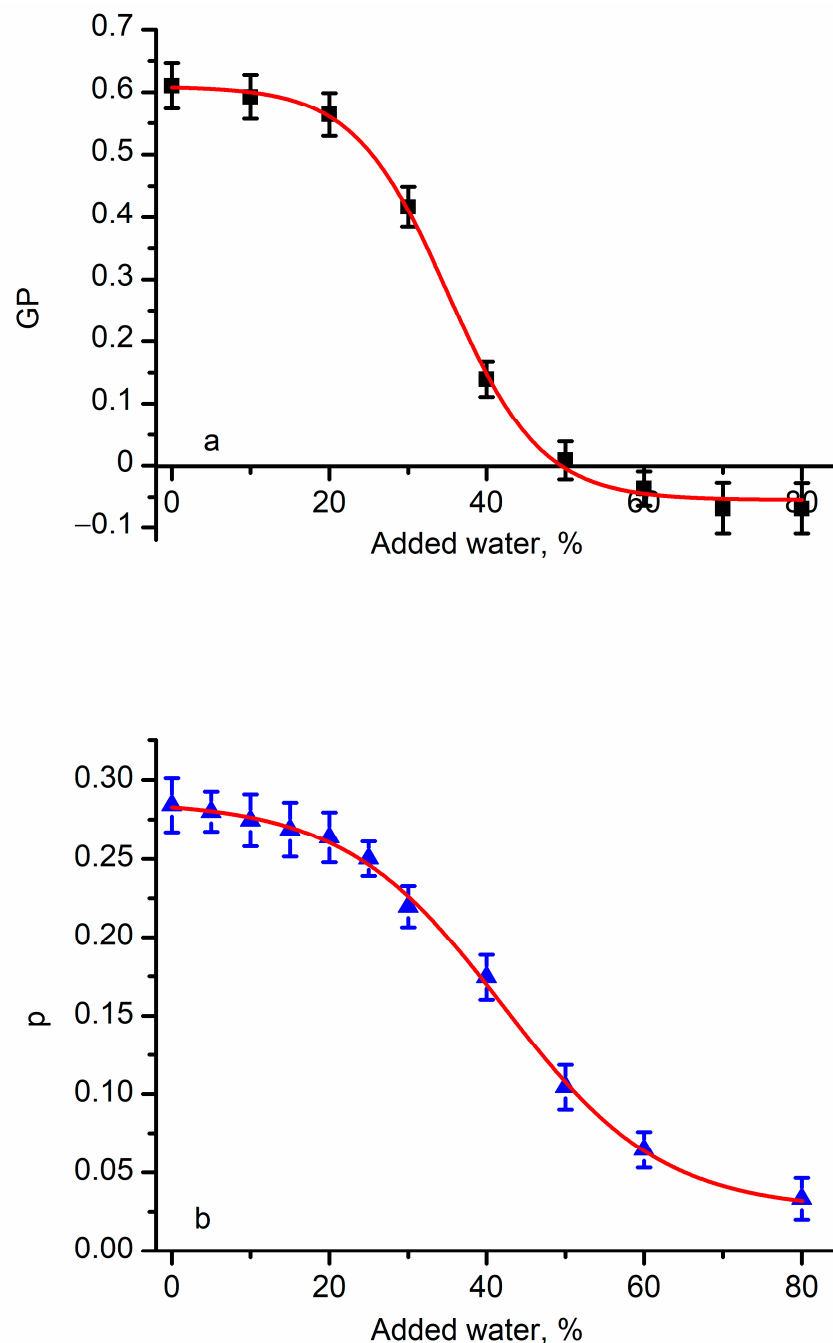


Figure 2. The optical response of membrane probe dyes residing in the membrane of RBCs is modulated by hypo-osmotic pressure and indicates changes in lipid ordering. The generalized polarization of Laurdan (a) and DPH's anisotropy (b) decreased in a sigmoidal fashion upon gradual exposure to hypo-osmotic shocks. The symbol represents average values \pm SD ($n = 3$); the red traces show the fit with the Boltzmann function, resembling phase transitions.

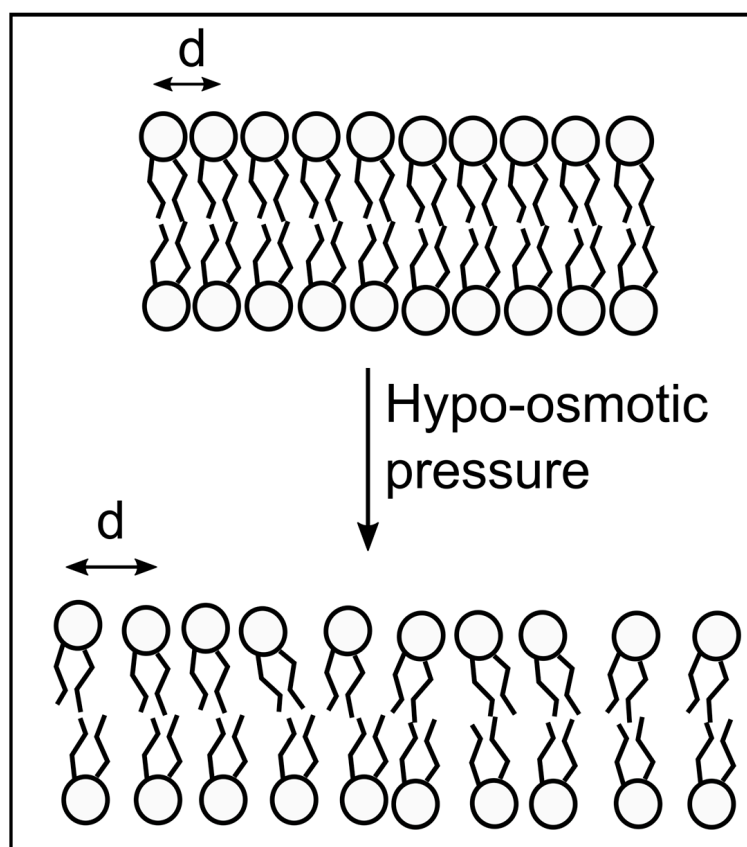


Figure 3. Proposed mechanism for the changes in lipid ordering elicited by membrane exposure to hypo-osmotic pressure. Under hypo-osmotic stress, the intermolecular distance d between neighboring lipid molecules increases. The short-range interactions between the membrane components are overcome by the membrane's tension induced by stretching, leading to decreased lipid ordering, greater fluidity, and accessible solvation.

The hypothesized changes in intermolecular distances and lipid ordering may explain water penetration, which adjusts the Laurdan's emission, and the effects on DPH's rotational diffusion. The rotational diffusion depends on the environment's viscosity and temperature; however, our experiments were performed at a constant temperature. Therefore, the increased intermolecular distances and less rigid membrane may allow faster adjustments of the DPH's orientation, hence modulating the anisotropy as observed in our experiments.

3.3. Pore-Forming Toxins (PFTs) Adjust the Lipid Order in Target Membranes

Next, we addressed the changes in lipid order induced by the insertion of two model PFTs, lysenin and SLO, into RBC membranes. The lysenin addition led to a gradual decrease in the GP values (Figure 4a), which was interpreted based on the Laurdan's ability to indicate lipid order, fluidity, and solvent exposure. The GP decreased significantly (from ~ 0.6 at 0 ng/mL of lysenin to ~ 0.1 at 3 ng/mL of lysenin) as lysenin's concentration increased, indicating that the addition of a toxin led to a faster dipolar relaxation. Similarly, the DPH's anisotropy decreased considerably (Figure 4b) from ~ 0.24 at 0 ng/mL of lysenin to ~ 0.02 at 0.6 ng/mL of lysenin. Both variations were larger than the ones induced by cholesterol depletion (Figure 1) and approached the changes measured for hypo-osmotic conditions (Figure 2), suggesting the occurrence of major changes in the RBCs' membrane status.

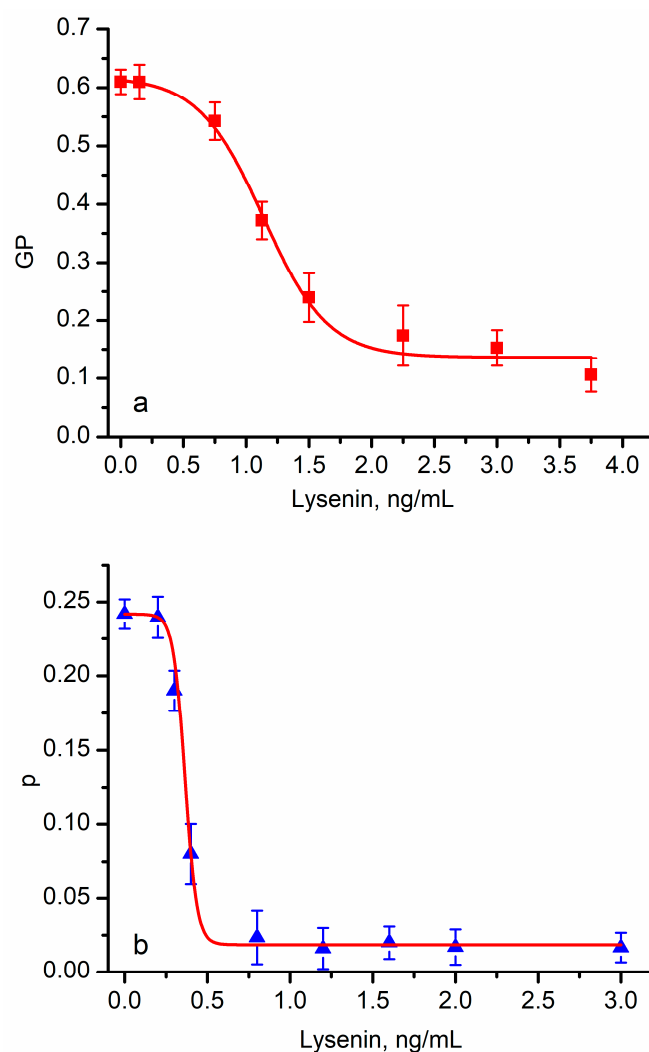


Figure 4. Lysenin insertion into RBC membranes decreases lipid ordering. The Laurdan's generalized polarization function (a) decreased upon lysenin addition in a concentration dependent manner, suggesting that channel insertion led to a reduced ordering of the lipids. A marked decrease was also encountered for DPH's anisotropy upon lysenin's insertion (b), supporting the hypothesis of changes in lipid ordering. Each symbol represents average experimental data \pm SD ($n = 3$), and the red traces show the fit with the Boltzmann function.

In addition to the larger variations in the optical responses, the exposure to lysenin led to sigmoidal-shaped curves, which were characteristic of phase transitions [26,28]. However, the visual analysis of the plots and the Boltzmann fit indicated a quantitative difference; the halfway concentration of lysenin (the inflex point) was different for the two dyes (i.e., ~ 1.1 ng/mL for Laurdan and ~ 0.4 ng/mL for DPH). DPH's anisotropy is a direct consequence of the rotational diffusion and, hence, a measure of fluidity. However, Laurdan's fluorescence stems from its dipolar relaxation, which may have multiple origins. For example, a local change in the lipid ordering by the inserted protein may have a more pronounced influence on the rotational diffusion than water penetration or dipolar relaxation. To further examine the influence presented by toxin insertion, we repeated the experiments by replacing lysenin with another potent pore-forming toxin, streptolysin O (SLO). Strong qualitative similarities between lysenin (Figure 4) and SLO (Figure 5) have been observed in regard to optical response. SLO addition also led to a decrease in generalized polarization and anisotropy in a concentration-dependent manner similar to our lysenin observations. In addition, the absolute changes in GP and anisotropy resembled the values determined for lysenin.

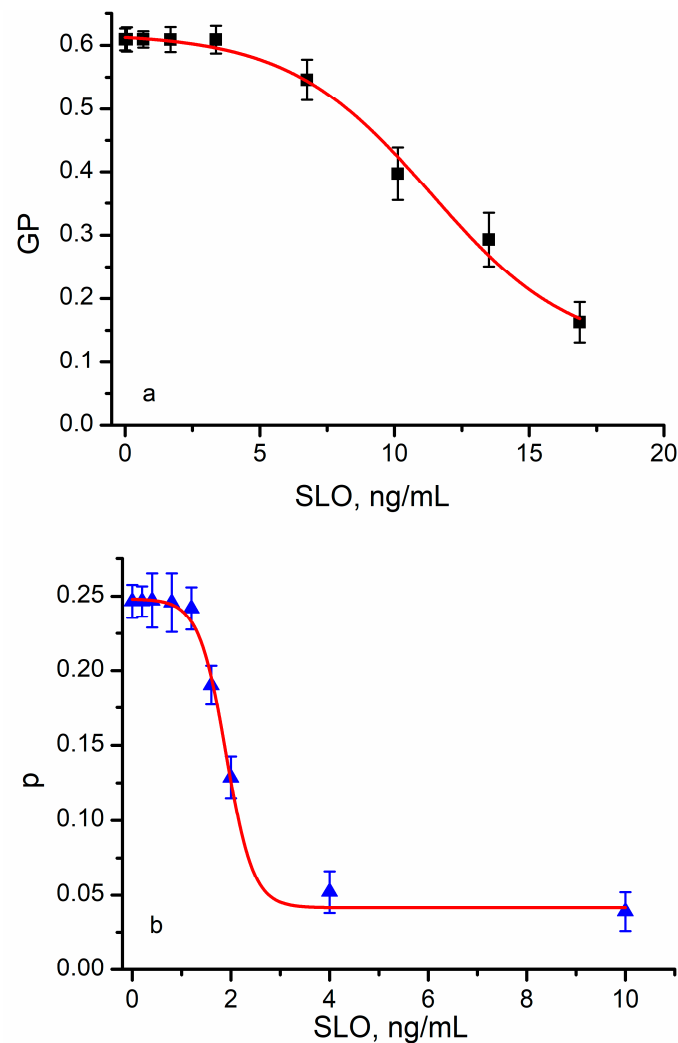


Figure 5. Streptolysin O (SLO) insertion into RBC membranes influences lipid ordering. Upon SLO insertion, Laurdan’s GP function decreased in a concentration-dependent manner (a), suggesting that channel insertion decreased ordering of the lipids. A marked decrease was also determined upon SLO’s insertion from DPH’s anisotropy (b), suggesting changes in lipid ordering. Each symbol represents average experimental data \pm SD ($n = 3$), and the red traces show the fit with the Boltzmann function.

The Laurdan’s response to SLO addition was smaller than the response prompted by lysenin, and a similar decrease in GP was determined for much larger SLO concentrations (i.e., ~ 16 ng/mL of SLO as opposed to ~ 3 ng/mL of lysenin). This large difference may not have been a consequence of SLO’s lower biological activity since DPH was more sensitive and showed an optical response similar to lysenin for the same concentration range (the minimum plateau was reached at ~ 4 ng SLO/mL). Although the sigmoidal shape of the anisotropy was obvious for DPH, Laurdan did not exhibit a strong sigmoidal curve. The inflection points determined from the fit were 11.32 ng/mL for Laurdan and 1.9 ng/mL for DPH. Both dyes are indicative of potential phase transitions occurring due to the protein–membrane interactions, which we exploited to provide a mechanistic view of the changes in membrane status upon exposure to PFTs.

The notable changes in the optical response and the sigmoidal behavior suggest that the RBC membranes exposed to PFTs undergo major changes at the molecular level. The functional pore is a result of many processes of primary interactions with channel-forming membrane components, such as cholesterol or sphingomyelin, and oligomerization [71–77]. Both toxins act quickly on target membranes; therefore, the time frame of the experiment al-

lowed for the full equilibration of each sample. No significant changes have been observed for either toxin at low concentrations. A low concentration of the toxins may not preclude interactions with the membranes, but it is uncertain if minimal changes in the optical response are a consequence of the poor sensitivity of the measuring method or the absence of insertion and pore formation. Both toxins elicited large variations in the optical response at high concentrations, which is indicative of notable changes in the membrane's environment. However, asymptotic behavior, irrespective of the optical probe and approaching a minimal value, was observed for lysenin. SLO presented this behavior only in the presence of DPH. We may not exclude the existence of a similar plateau for the SLO/Laurdan system at SLO concentrations greater than those used in our study. These quantitative and qualitative differences may be explained by accounting for different biological activities (i.e., affinities for target membranes) and the mechanisms of action for the two toxins (i.e., a different mechanism of oligomerization, pre-pore formation, binding to lipid components, and insertion). Nonetheless, major changes in the optical responses were triggered for both toxins at certain concentrations.

An explanation of the sudden changes induced by the toxin's insertion into target RBC membranes is the consideration of boundary conditions at the lipid-protein interface. Inclusions into membranes may manifest by midplane bending, torsional effects, or hydrophobic mismatches [70,78–83]. Among these, the structural data of SLO and lysenin [74,84–86] suggest that a hydrophobic mismatch leads to the observed changes in generalized polarization and anisotropy. At a low protein concentration, the center-to-center distance between inserted proteins is large. Consequently, substantial membrane deformation may be limited to the immediate region surrounding the inserted protein [70,79–81] (Figure 6). This insertion-induced membrane curvature manifests at a short-length scale, and the lipid order is disturbed only within the small volume surrounding the inserted channel. In this small volume, solvent penetration and dipolar relaxation are limited. As opposed to DPH, which undergoes enhanced rotational diffusion in the vicinity of the protein, Laurdan's relaxation may not benefit from hydration, explaining the weaker response. To explain the large differences in the Laurdan's response to lysenin and SLO, we may consider the different geometries of the inserted proteins and the different interactions with membrane's components. Lysenin's oligomerization and subsequent pore formation requires a primary interaction with sphingomyelin [72,73,85], while SLO binds to the cholesterol molecules inside the membrane [76,77,87]. Consequently, SLO may sequester cholesterol molecules around the inserted channel, preventing major lipid disordering, a decrease in fluidity, and water penetration, thus weakening the optical response to SLO insertion. This effect should also influence the rotational diffusion of DPH, which is suggested by the slightly reduced response elicited upon exposure to SLO in comparison to lysenin.

The weaker response presented by Laurdan in the presence of SLO may also be explained by a higher local concentration of cholesterol upon sequestration. The increased rigidity of the membrane may reduce the lipid motion and prevent water penetration, a major mechanism of Laurdan's dipolar relaxation. However, higher densities of reconstituted proteins may further contribute to substantial changes in the membrane's geometry. At reduced center-to-center distances, the curved surfaces may coalesce [70,80,81], leading to larger deformations of the membrane, a global increase in the membrane thickness, greater lipid disorder, and a larger portion of the membrane being prone to solvent penetration. The SLO data are in agreement with tube extrusion experiments that show a loss of the elasticity of SLO's permeabilized membranes [88]. To explain the differences between SLO and lysenin data, one may consider the lysenin's preference for insertion into lipid rafts [72,89], which may lead to much higher local densities of proteins in the target membranes.

An additional observation can be made regarding the initial values of GP and p parameters. While these values are consistent with prior reports, the initial anisotropy parameter underwent large variations, while the GP value remained practically the same. One may assume that this experimental variability may originate in the "aging" of RBCs preserved in vitro and our inability to perform all the experiments in a short period of time.

Because only anisotropy exhibited large variations, it suggests that the optical responses from the two dyes are not highly correlated. This assumption is reasonable since the two dyes, although sparingly used to assess lipid ordering, respond to different membrane conditions (i.e., dipolar relaxation as opposed to fluidity).

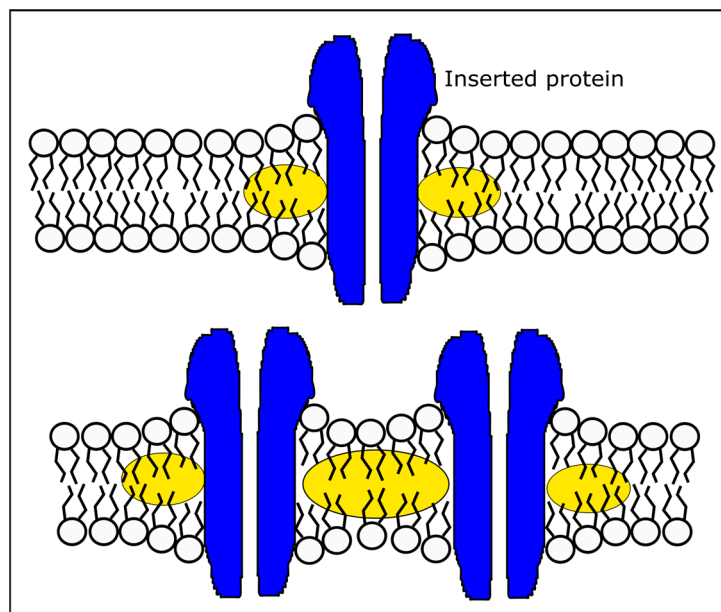


Figure 6. Proposed hydrophobic mismatch mechanism for changes in lipid ordering induced by insertion of pore-forming toxins (PFTs) into target membranes. At low PFT concentrations (**top**), the hydrophobic mismatch locally affects the lipid ordering within a small region surrounding the inserted protein (highlighted ellipses); consequently, the changes in lipid ordering are spatially limited. At high PFT concentration (**bottom**), the inter-channel region is also affected, the disordered volume increases significantly and leads to larger adjustments in dipolar relaxation and rotational diffusion of environmentally sensitive probes.

In conclusion, our experiments show that Laurdan and DPH may be used to assess changes in the membrane status induced by hypo-osmotic pressure or the insertion of transmembrane proteins. For both environmental conditions, the variations in the optical response resemble transitions between liquid-ordered and liquid-disordered phases. While such transitions are typically encountered in response to variations in temperature, our results show that they may occur at constant temperature under the influence of mechanical or biological stimulation. We related the presumed phase transitions to the disorganization of the lipids and short-range interactions in the membrane modulated by mechanical stress elicited by hypoosmotic shocks or hydrophobic mismatches in the target membranes. Nonetheless, further work is needed to concretely establish that the observed changes are consequences of true phase transitions in the membranes. Therefore, this work may lead to a better understanding of how cells respond to physical, chemical, or biological environmental stimulations.

Supplementary Materials: The following supporting information can be downloaded at: <https://www.mdpi.com/article/10.3390/membranes13070620/s1>, Figure S1: Intact membranes are indicated by fluorescence microscopy.

Author Contributions: Conceptualization, D.F. and R.W.; methodology, R.W., D.F., S.S., M.K., M.P. and D.R.; formal analysis, R.W., D.F., D.R., J.K., M.P., A.R.S. and Z.L.; investigation, D.F., R.W., M.P., M.K., A.R.S., S.S., D.R., J.K. and Z.L.; validation, R.W., M.K., M.P., A.R.S., S.S., D.R., Z.L. and J.K.; resources, D.F.; supervision, D.F. and R.W. All authors contributed to the original draft preparation, review, and editing. All authors have read and agreed to the published version of the manuscript.

Funding: This research was funded by the National Science Foundation (grant number 1554166), National Institute of Health (grant numbers P20GM103408 and P20GM109095), and National Institutes of General Medical Science's Centers of Biomedical Research Excellence program grant number P20GM109007.

Institutional Review Board Statement: Not applicable.

Data Availability Statement: The data presented in this study are available on request from the corresponding author.

Conflicts of Interest: The authors declare no conflict of interest. The funding agencies had no role in the design of the study; in the collection, analyses, or interpretation of data; in the writing of the manuscript; or in the decision to publish the results.

References

1. Suzuki, K.G.N.; Kusumi, A. Refinement of Singer-Nicolson fluid-mosaic model by microscopy imaging: Lipid rafts and actin-induced membrane compartmentalization. *Biochim. Biophys. Acta Biomembr.* **2023**, *1865*, 184093. [[CrossRef](#)] [[PubMed](#)]
2. Jouhet, J. Importance of the hexagonal lipid phase in biological membrane organization. *Front. Plant. Sci.* **2013**, *4*, 494. [[CrossRef](#)]
3. Goñi, F.M. The basic structure and dynamics of cell membranes: An update of the Singer-Nicolson model. *Biochim. Biophys. Acta* **2014**, *1838*, 1467–1476. [[CrossRef](#)] [[PubMed](#)]
4. Kaiser, H.-J.; Lingwood, D.; Levental, I.; Sampaio, J.L.; Kalvodova, L.; Rajendran, L.; Simons, K. Order of lipid phases in model and plasma membranes. *Proc. Natl. Acad. Sci. USA* **2009**, *106*, 16645–16650. [[CrossRef](#)] [[PubMed](#)]
5. Klymchenko, A.S.; Kreder, R. Fluorescent Probes for Lipid Rafts: From Model Membranes to Living Cells. *Chem. Biol.* **2014**, *21*, 97–113. [[CrossRef](#)]
6. Nicolson, G.L. Update of the 1972 Singer-Nicolson Fluid-Mosaic Model of Membrane Structure. *Discoveries* **2013**, *1*, e3. [[CrossRef](#)]
7. Simons, K.; Ikonen, E. Functional rafts in cell membranes. *Nature* **1997**, *387*, 569–572. [[CrossRef](#)]
8. Shaw, T.R.; Ghosh, S.; Veatch, S.L. Critical Phenomena in Plasma Membrane Organization and Function. *Annu. Rev. Phys. Chem.* **2021**, *72*, 51–72. [[CrossRef](#)]
9. Lingwood, D.; Simons, K. Lipid Rafts As a Membrane-Organizing Principle. *Science* **2010**, *327*, 46–50. [[CrossRef](#)]
10. London, E. Insights into lipid raft structure and formation from experiments in model membranes. *Curr. Opin. Struct. Biol.* **2002**, *12*, 480–486. [[CrossRef](#)]
11. London, E. Ordered Domain (Raft) Formation in Asymmetric Vesicles and Its Induction upon Loss of Lipid Asymmetry in Artificial and Natural Membranes. *Membranes* **2022**, *12*, 870. [[CrossRef](#)]
12. Murata, M.; Matsumori, N.; Kinoshita, M.; London, E. Molecular substructure of the liquid-ordered phase formed by sphingomyelin and cholesterol: Sphingomyelin clusters forming nano-subdomains are a characteristic feature. *Biophys. Rev.* **2022**, *14*, 655–678. [[CrossRef](#)]
13. Gaibelet, G.; Tercé, F.; Allart, S.; Lebrun, C.; Collet, X.; Jamin, N.; Orłowski, S. Fluorescent probes for detecting cholesterol-rich ordered membrane microdomains: Entangled relationships between structural analogies in the membrane and functional homologies in the cell. *AIMS Biophys.* **2017**, *4*, 121–151. [[CrossRef](#)]
14. Gibbons, E.; Pickett, K.R.; Streeter, M.C.; Warcup, A.O.; Nelson, J.; Judd, A.M.; Bell, J.D. Molecular details of membrane fluidity changes during apoptosis and relationship to phospholipase A2 activity. *Biochim. Biophys. Acta* **2013**, *1828*, 887–895. [[CrossRef](#)]
15. Bálint, Š.; Dustin, M.L. Localizing order to boost signaling. *Elife* **2017**, *6*, e25375. [[CrossRef](#)]
16. Dustin, M.L.; Muller, J. Liquidity in immune cell signaling. *Science* **2016**, *352*, 516–517. [[CrossRef](#)]
17. Stone, M.B.; Shelby, S.A.; Núñez, M.F.; Wissner, K.; Veatch, S.L. Protein sorting by lipid phase-like domains supports emergent signaling function in B lymphocyte plasma membranes. *eLife* **2017**, *6*, e19891. [[CrossRef](#)]
18. Su, X.; Ditlev, J.A.; Hui, E.; Xing, W.; Banjade, S.; Okrut, J.; King, D.S.; Taunton, J.; Rosen, M.K.; Vale, R.D. Phase separation of signaling molecules promotes T cell receptor signal transduction. *Science* **2016**, *352*, 595–599. [[CrossRef](#)]
19. Noutsis, P.; Gratton, E.; Chaieb, S. Assessment of Membrane Fluidity Fluctuations during Cellular Development Reveals Time and Cell Type Specificity. *PLoS ONE* **2016**, *11*, e0158313. [[CrossRef](#)]
20. Gupta, A.; Dey, S.; Bhowmik, D.; Maiti, S. Coexisting Ordered and Disordered Membrane Phases Have Distinct Modes of Interaction with Disease-Associated Oligomers. *J. Phys. Chem. B* **2022**, *126*, 1016–1023. [[CrossRef](#)]
21. Gimpl, G.; Fahrenholz, F. Human oxytocin receptors in cholesterol-rich vs. cholesterol-poor microdomains of the plasma membrane. *Eur. J. Biochem.* **2000**, *267*, 2483–2497. [[CrossRef](#)]
22. Urbančič, I.; Schiffelers, L.; Jenkins, E.; Gong, W.; Santos, A.M.; Schneider, F.; O'Brien-Ball, C.; Vuong, M.T.; Ashman, N.; Sezgin, E.; et al. Aggregation and mobility of membrane proteins interplay with local lipid order in the plasma membrane of T cells. *FEBS Lett.* **2021**, *595*, 2127–2146. [[CrossRef](#)]
23. Gonzalez, L.J.; Gibbons, E.; Bailey, R.W.; Fairbourn, J.; Nguyen, T.; Smith, S.K.; Best, K.B.; Nelson, J.; Judd, A.M.; Bell, J.D. The influence of membrane physical properties on microvesicle release in human erythrocytes. *PMC Biophys.* **2009**, *2*, 7. [[CrossRef](#)]
24. Sengupta, S.; Karsalia, R.; Morrissey, A.; Bamezai, A.K. Cholesterol-dependent plasma membrane order (Lo) is critical for antigen-specific clonal expansion of CD4+ T cells. *Sci. Rep.* **2021**, *11*, 13970. [[CrossRef](#)]

25. Orlikowska-Rzeznik, H.; Krok, E.; Chattopadhyay, M.; Lester, A.; Piatkowski, L. Laurdan discerns lipid membrane hydration and cholesterol content. *bioRxiv* **2022**, *2022*, 514927. [[CrossRef](#)]
26. Färber, N.; Westerhausen, C. Broad lipid phase transitions in mammalian cell membranes measured by Laurdan fluorescence spectroscopy. *Biochim. Biophys. Acta* **2022**, *1864*, 183794. [[CrossRef](#)]
27. Neunert, G.; Tomaszewska-Gras, J.; Baj, A.; Gauza-Włodarczyk, M.; Witkowski, S.; Polewski, K. Phase Transitions and Structural Changes in DPPC Liposomes Induced by a 1-Carba-Alpha-Tocopherol Analogue. *Molecules* **2021**, *26*, 2851. [[CrossRef](#)]
28. Havlíková, M.; Szabová, J.; Mravcová, L.; Venerová, T.; Chang, C.-H.; Pekař, M.; Jugl, A.; Mravec, F. Cholesterol Effect on Membrane Properties of Cationic Ion Pair Amphiphile Vesicles at Different Temperatures. *Langmuir* **2021**, *37*, 2436–2444. [[CrossRef](#)]
29. Kure, T.; Sakai, H. Transmembrane Difference in Colloid Osmotic Pressure Affects the Lipid Membrane Fluidity of Liposomes Encapsulating a Concentrated Protein Solution. *Langmuir* **2017**, *33*, 1533–1540. [[CrossRef](#)]
30. Bagatolli, L.A.; Maggio, B.; Aguilar, F.; Sotomayor, C.P.; Fidelio, G.D. Laurdan properties in glycosphingolipid-phospholipid mixtures: A comparative fluorescence and calorimetric study. *Biochim. Biophys. Acta* **1997**, *1325*, 80–90. [[CrossRef](#)]
31. Parasassi, T.; Di Stefano, M.; Loiero, M.; Ravagnan, G.; Gratton, E. Influence of cholesterol on phospholipid bilayers phase domains as detected by Laurdan fluorescence. *Biophys. J.* **1994**, *66*, 120–132. [[CrossRef](#)]
32. Parasassi, T.; De Stasio, G.; Ravagnan, G.; Rusch, R.M.; Gratton, E. Quantitation of lipid phases in phospholipid vesicles by the generalized polarization of Laurdan fluorescence. *Biophys. J.* **1991**, *60*, 179–189. [[CrossRef](#)]
33. Moulton, E.R.; Hirsche, K.J.; Hobbs, M.L.; Schwab, J.M.; Bailey, E.G.; Bell, J.D. Examining the effects of cholesterol on model membranes at high temperatures: Laurdan and Patman see it differently. *Biochim. Biophys. Acta* **2018**, *1860*, 1571–1579. [[CrossRef](#)]
34. Pokorna, S.; Ventura, A.E.; Santos, T.C.B.; Hof, M.; Prieto, M.; Futerman, A.H.; Silva, L.C. Laurdan in live cell imaging: Effect of acquisition settings, cell culture conditions and data analysis on generalized polarization measurements. *J. Photochem. Photobiol. B Biol.* **2022**, *228*, 112404. [[CrossRef](#)]
35. Zhang, Y.-L.; Frangos, J.A.; Chachisvilis, M. Laurdan fluorescence senses mechanical strain in the lipid bilayer membrane. *Biochem. Biophys. Res. Commun.* **2006**, *347*, 838–841. [[CrossRef](#)]
36. do Canto, A.M.T.M.; Robalo, J.R.; Santos, P.D.; Carvalho, A.J.P.; Ramalho, J.P.P.; Loura, L.M.S. Diphenylhexatriene membrane probes DPH and TMA-DPH: A comparative molecular dynamics simulation study. *Biochim. Biophys. Acta* **2016**, *1858*, 2647–2661. [[CrossRef](#)]
37. Mykytczuk, N.C.S.; Trevors, J.T.; Leduc, L.G.; Ferroni, G.D. Fluorescence polarization in studies of bacterial cytoplasmic membrane fluidity under environmental stress. *Prog. Biophys. Mol. Biol.* **2007**, *95*, 60–82. [[CrossRef](#)]
38. Bondelli, G.; Paternò, G.M.; Lanzani, G. Fluorescent probes for optical investigation of the plasma membrane. *Opt. Mater. X* **2021**, *12*, 100085. [[CrossRef](#)]
39. Sanchez, S.A.; Tricerri, M.A.; Gratton, E. Laurdan generalized polarization fluctuations measures membrane packing micro-heterogeneity in vivo. *Proc. Natl. Acad. Sci. USA* **2012**, *109*, 7314–7319. [[CrossRef](#)]
40. Ariola, F.S.; Li, Z.; Cornejo, C.; Bittman, R.; Heikal, A.A. Membrane Fluidity and Lipid Order in Ternary Giant Unilamellar Vesicles Using a New Bodipy-Cholesterol Derivative. *Biophys. J.* **2009**, *96*, 2696–2708. [[CrossRef](#)]
41. Blicher, A.; Wodzinska, K.; Fidorra, M.; Winterhalter, M.; Heimburg, T. The Temperature Dependence of Lipid Membrane Permeability, its Quantized Nature, and the Influence of Anesthetics. *Biophys. J.* **2009**, *96*, 4581–4591. [[CrossRef](#)]
42. Frallicciardi, J.; Melcr, J.; Siginou, P.; Marrink, S.J.; Poolman, B. Membrane thickness, lipid phase and sterol type are determining factors in the permeability of membranes to small solutes. *Nat. Commun.* **2022**, *13*, 1605. [[CrossRef](#)] [[PubMed](#)]
43. Kraske, W.V.; Mountcastle, D.B. Effects of cholesterol and temperature on the permeability of dimyristoylphosphatidylcholine bilayers near the chain melting phase transition. *Biochim. Biophys. Acta* **2001**, *1514*, 159–164. [[CrossRef](#)]
44. Ma, Y.; Benda, A.; Kwiatek, J.; Owen, D.M.; Gaus, K. Time-Resolved Laurdan Fluorescence Reveals Insights into Membrane Viscosity and Hydration Levels. *Biophys. J.* **2018**, *115*, 1498–1508. [[CrossRef](#)] [[PubMed](#)]
45. Pan, J.; Tristram-Nagle, S.; Kučerka, N.; Nagle, J.F. Temperature Dependence of Structure, Bending Rigidity, and Bilayer Interactions of Dioleoylphosphatidylcholine Bilayers. *Biophys. J.* **2008**, *94*, 117–124. [[CrossRef](#)]
46. Steinkühler, J.; Sezgin, E.; Urbančič, I.; Eggeling, C.; Dimova, R. Mechanical properties of plasma membrane vesicles correlate with lipid order, viscosity and cell density. *Commun. Biol.* **2019**, *2*, 337. [[CrossRef](#)]
47. Hamada, N.; Longo, M.L. Characterization of phase separation phenomena in hybrid lipid/block copolymer/cholesterol bilayers using laurdan fluorescence with log-normal multipeak analysis. *Biochim. Biophys. Acta* **2022**, *1864*, 183887. [[CrossRef](#)]
48. Stott, B.M.; Vu, M.P.; McLemore, C.O.; Lund, M.S.; Gibbons, E.; Brueseke, T.J.; Wilson-Ashworth, H.A.; Bell, J.D. Use of fluorescence to determine the effects of cholesterol on lipid behavior in sphingomyelin liposomes and erythrocyte membranes. *J. Lipid Res.* **2008**, *49*, 1202–1215. [[CrossRef](#)]
49. Ingólfsson, H.I.; Melo, M.N.; van Eerden, F.J.; Arnarez, C.; Lopez, C.A.; Wassenaar, T.A.; Periolo, X.; de Vries, A.H.; Tieleman, D.P.; Marrink, S.J. Lipid Organization of the Plasma Membrane. *J. Am. Chem. Soc.* **2014**, *136*, 14554–14559. [[CrossRef](#)]
50. Luchini, A.; Vitiello, G. Mimicking the Mammalian Plasma Membrane: An Overview of Lipid Membrane Models for Biophysical Studies. *Biomimetics* **2021**, *6*, 3. [[CrossRef](#)]
51. Róg, T.; Pasenkiewicz-Gierula, M.; Vattulainen, I.; Karttunen, M. Ordering effects of cholesterol and its analogues. *Biochim. Biophys. Acta* **2009**, *1788*, 97–121. [[CrossRef](#)]

52. de Meyer, F.; Smit, B. Effect of cholesterol on the structure of a phospholipid bilayer. *Proc. Natl. Acad. Sci. USA* **2009**, *106*, 3654–3658. [[CrossRef](#)]
53. Los, D.A.; Murata, N. Membrane fluidity and its roles in the perception of environmental signals. *Biochim. Biophys. Acta* **2004**, *1666*, 142–157. [[CrossRef](#)] [[PubMed](#)]
54. Söderlund, T.; Alakoskela, J.-M.I.; Pakkanen, A.L.; Kinnunen, P.K.J. Comparison of the Effects of Surface Tension and Osmotic Pressure on the Interfacial Hydration of a Fluid Phospholipid Bilayer. *Biophys. J.* **2003**, *85*, 2333–2341. [[CrossRef](#)] [[PubMed](#)]
55. Nomoto, T.; Takahashi, M.; Fujii, T.; Chiari, L.; Toyota, T.; Fujinami, M. Effects of Cholesterol Concentration and Osmolarity on the Fluidity and Membrane Tension of Free-standing Black Lipid Membranes. *Anal. Sci.* **2018**, *34*, 1237–1242. [[CrossRef](#)]
56. Laroche, C.; Beney, L.; Marechal, P.; Gervais, P. The effect of osmotic pressure on the membrane fluidity of *Saccharomyces cerevisiae* at different physiological temperatures. *Appl. Microbiol. Biotechnol.* **2001**, *56*, 249–254. [[CrossRef](#)]
57. Bogard, A.; Finn, P.W.; McKinney, F.; Flacau, I.M.; Smith, A.R.; Whiting, R.; Fologea, D. The Ionic Selectivity of Lysenin Channels in Open and Sub-Conducting States. *Membranes* **2021**, *11*, 897. [[CrossRef](#)]
58. Amaro, M.; Reina, F.; Hof, M.; Eggeling, C.; Sezgin, E. Laurdan and Di-4-ANEPPDHQ probe different properties of the membrane. *J. Phys. D: Appl. Phys.* **2017**, *50*, 134004. [[CrossRef](#)]
59. Weber, P.; Wagner, M.; Schneckenburger, H. Fluorescence imaging of membrane dynamics in living cells. *J. Biomed. Opt.* **2010**, *15*, 046017. [[CrossRef](#)]
60. Golfetto, O.; Hinde, E.; Gratton, E. Laurdan Fluorescence Lifetime Discriminates Cholesterol Content from Changes in Fluidity in Living Cell Membranes. *Biophys. J.* **2013**, *104*, 1238–1247. [[CrossRef](#)]
61. Horváth, Á.; Erostyák, J.; Szóke, É. Effect of Lipid Raft Disruptors on Cell Membrane Fluidity Studied by Fluorescence Spectroscopy. *Int. J. Mol. Sci.* **2022**, *23*, 13729. [[CrossRef](#)]
62. dos Santos, A.G.; Bayiha, J.C.; Dufour, G.; Cataldo, D.; Evrard, B.; Silva, L.C.; Deleu, M.; Mingeot-Leclercq, M.-P. Changes in membrane biophysical properties induced by the Budesonide/Hydroxypropyl- β -cyclodextrin complex. *Biochim. Biophys. Acta* **2017**, *1859*, 1930–1940. [[CrossRef](#)]
63. Xü, Y.H.; Gietzen, K.; Galla, H.J.; Sackmann, E. A simple assay to study protein-mediated lipid exchange by fluorescence polarization. *Biochem. J.* **1983**, *209*, 257–260. [[CrossRef](#)]
64. Nagamachi, E.; Hirai, Y.; Tomochika, K.; Kanemasa, Y. Studies on Osmotic Stability of Liposomes Prepared with Bacterial Membrane Lipids by Carboxyfluorescein Release. *Microbiol. Immunol.* **1992**, *36*, 231–241. [[CrossRef](#)]
65. Reddy, A.S.; Warshaviak, D.T.; Chachisvilis, M. Effect of membrane tension on the physical properties of DOPC lipid bilayer membrane. *Biochim. Biophys. Acta* **2012**, *1818*, 2271–2281. [[CrossRef](#)] [[PubMed](#)]
66. Anderson, P.C.; Lovrien, R.E. Human red cell hemolysis rates in the subsecond to seconds range. An analysis. *Biophys. J.* **1977**, *20*, 181–191. [[CrossRef](#)] [[PubMed](#)]
67. Johnson, R.M.; Taylor, G.; Meyer, D.B. Shape and volume changes in erythrocyte ghosts and spectrin-actin networks. *J. Cell Biol.* **1980**, *86*, 371–376. [[CrossRef](#)] [[PubMed](#)]
68. Beattie, M.E.; Veatch, S.L.; Stottrup, B.L.; Keller, S.L. Sterol Structure Determines Miscibility versus Melting Transitions in Lipid Vesicles. *Biophys. J.* **2005**, *89*, 1760–1768. [[CrossRef](#)]
69. Boyd, M.A.; Kamat, N.P. Visualizing Tension and Growth in Model Membranes Using Optical Dyes. *Biophys. J.* **2018**, *115*, 1307–1315. [[CrossRef](#)] [[PubMed](#)]
70. Phillips, R.; Ursell, T.; Wiggins, P.; Sens, P. Emerging roles for lipids in shaping membrane-protein function. *Nature* **2009**, *459*, 379–385. [[CrossRef](#)] [[PubMed](#)]
71. Ide, T.; Aoki, T.; Takeuchi, Y.; Yanagida, T. Lysenin forms a voltage-dependent channel in artificial lipid bilayer membranes. *Biochem. Biophys. Res. Commun.* **2006**, *346*, 288–292. [[CrossRef](#)] [[PubMed](#)]
72. Kulma, M.; Herec, M.; Grudziński, W.; Anderluh, G.; Gruszecki, W.I.; Kwiatkowska, K.; Sobota, A. Sphingomyelin-rich domains are sites of lysenin oligomerization: Implications for raft studies. *Biochim. Biophys. Acta* **2010**, *1798*, 471–481. [[CrossRef](#)]
73. Yilmaz, N.; Yamaji-Hasegawa, A.; Hullin-Matsuda, F.; Kobayashi, T. Molecular mechanisms of action of sphingomyelin-specific pore-forming toxin, lysenin. *Semin. Cell Dev. Biol.* **2018**, *73*, 188–198. [[CrossRef](#)] [[PubMed](#)]
74. Feil, S.C.; Ascher, D.B.; Kuiper, M.J.; Tweten, R.K.; Parker, M.W. Structural Studies of *Streptococcus pyogenes* Streptolysin O Provide Insights into the Early Steps of Membrane Penetration. *J. Mol. Biol.* **2014**, *426*, 785–792. [[CrossRef](#)]
75. Miller, H.; Song, W. Use of Streptolysin O-Induced Membrane Damage as a Method of Studying the Function of Lipid Rafts During B Cell Activation. In *B Cell Receptor Signaling: Methods and Protocols*; Liu, C., Ed.; Springer: New York, NY, USA, 2018; pp. 235–241.
76. Tweten, R.K.; Hotze, E.M.; Wade, K.R. The Unique Molecular Choreography of Giant Pore Formation by the Cholesterol-Dependent Cytolysins of Gram-Positive Bacteria. *Annu. Rev. Microbiol.* **2015**, *69*, 323–340. [[CrossRef](#)]
77. Giddings, K.S.; Johnson, A.E.; Tweten, R.K. Redefining cholesterol's role in the mechanism of the cholesterol-dependent cytolysins. *Proc. Natl. Acad. Sci. USA* **2003**, *100*, 11315. [[CrossRef](#)] [[PubMed](#)]
78. Andersen, O.S.; Koeppe, R.E. Bilayer Thickness and Membrane Protein Function: An Energetic Perspective. *Annu. Rev. Biophys. Biomol. Struct.* **2007**, *36*, 107–130. [[CrossRef](#)]
79. Bavi, O.; Vossoughi, M.; Naghdabadi, R.; Jamali, Y. The Combined Effect of Hydrophobic Mismatch and Bilayer Local Bending on the Regulation of Mechanosensitive Ion Channels. *PLoS ONE* **2016**, *11*, e0150578. [[CrossRef](#)] [[PubMed](#)]

80. Gahbauer, S.; Böckmann, R.A. Membrane-Mediated Oligomerization of G Protein Coupled Receptors and Its Implications for GPCR Function. *Front. Physiol.* **2016**, *7*, 494. [[CrossRef](#)]
81. Kondrashov, O.V.; Kuzmin, P.I.; Akimov, S.A. Hydrophobic Mismatch Controls the Mode of Membrane-Mediated Interactions of Transmembrane Peptides. *Membranes* **2022**, *12*, 89. [[CrossRef](#)]
82. Piknova, B.; Perochon, E.; Tocanne, J.-F. Hydrophobic mismatch and long-range protein/lipid interactions in bacteriorhodopsin/phosphatidylcholine vesicles. *Eur. J. Biochem.* **1993**, *218*, 385–396. [[CrossRef](#)] [[PubMed](#)]
83. Startek, J.B.; Boonen, B.; Talavera, K.; Meseguer, V. TRP Channels as Sensors of Chemically-Induced Changes in Cell Membrane Mechanical Properties. *Int. J. Mol. Sci.* **2019**, *20*, 371. [[CrossRef](#)] [[PubMed](#)]
84. Bokori-Brown, M.; Martin, T.G.; Naylor, C.E.; Basak, A.K.; Titball, R.W.; Savva, C.G. Cryo-EM structure of lysenin pore elucidates membrane insertion by an aerolysin family protein. *Nat. Commun.* **2016**, *7*, 11293. [[CrossRef](#)] [[PubMed](#)]
85. De Colibus, L.; Sonnen, A.F.P.; Morris, K.J.; Siebert, A.C.; Abrusci, P.; Plitzko, J.; Hodnik, V.; Leippe, M.; Volpi, E.; Anderluh, G.; et al. Structures of lysenin reveal a shared evolutionary origin for pore-forming proteins and its mode of sphingomyelin recognition. *Structure* **2012**, *20*, 1498–1507. [[CrossRef](#)] [[PubMed](#)]
86. Podobnik, M.; Savory, P.; Rojko, N.; Kisovec, M.; Wood, N.; Hambley, R.; Pugh, J.; Wallace, E.J.; McNeill, L.; Bruce, M.; et al. Crystal structure of an invertebrate cytolysin pore reveals unique properties and mechanism of assembly. *Nat. Commun.* **2016**, *7*, 11598. [[CrossRef](#)]
87. Tweten, R.K. Cholesterol-Dependent Cytolysins, a Family of Versatile Pore-Forming Toxins. *Infect. Immun.* **2005**, *73*, 6199. [[CrossRef](#)]
88. Borghi, N.; Kremer, S.; Askovic, V.; Brochard-Wyart, F. Tube extrusion from permeabilized giant vesicles. *Europhys. Lett.* **2006**, *75*, 666. [[CrossRef](#)]
89. Krueger, E.; Bryant, S.; Shrestha, N.; Clark, T.; Hanna, C.; Pink, D.; Fologea, D. Intramembrane congestion effects on lysenin channel voltage-induced gating. *Eur. Biophys. J.* **2016**, *45*, 187–194. [[CrossRef](#)]

Disclaimer/Publisher's Note: The statements, opinions and data contained in all publications are solely those of the individual author(s) and contributor(s) and not of MDPI and/or the editor(s). MDPI and/or the editor(s) disclaim responsibility for any injury to people or property resulting from any ideas, methods, instructions or products referred to in the content.